Available online at www.sciencedirect.com
ScienceDirect
Journal of the European Ceramic Society 29 (2009) 611–619
www.elsevier.com/locate/jeurceramsoc

Thermal and physical characterisation of apatite/wollastonite bioactive glass–ceramics

Valeria Cannillo [a], Fiorenza Pierli [a], Sanjay Sampath [b], Cristina Siligardi [a,*]

[a] *Dipartimento di Ingegneria dei Materiali e dell'Ambiente, Università di Modena e Reggio Emilia, Via Vignolese 905, 41100 Modena, Italy*

[b] *Center for Thermal Spray Research, State University of New York, Stony Brook, NY 11784-2275, United States*

Received 24 April 2008; received in revised form 9 June 2008; accepted 20 June 2008
Available online 5 September 2008

Abstract

Glass–ceramics, containing apatite and wollastonite (A/W) crystals in the MgO–CaO–SiO_2–P_2O_5 glassy matrix, show the ability to form tight chemical bonds with living tissues when implanted in the body, as demonstrated by Kokubo and co-workers. However, the medical applications are mainly limited to non-load bearing conditions because of their poor mechanical properties. To overcome this drawback, a coating of the A/W glass–ceramic could be deposited onto a titanium substrate, in order to combine the good bioactivity of the bioceramic and the good mechanical strength of the titanium alloy base material. In this study, A/W powders obtained from commercial raw materials were thermally sprayed by APS (atmospheric plasma spraying) on Ti–6Al–4V substrates. Since in the as-sprayed conditions the coating microstructure was defective because of pores and cracks, thermal treatments on A/W plasma-sprayed coatings were conducted to enhance the coating microstructure. In order to gain a deeper insight, A/W bulk and sintered samples of the same composition were prepared and subjected to the same thermal treatments. In addition, the crystallisation behaviour of A/W bioactive glass–ceramic was investigated. The frits thermal behaviour was characterised by means of hot stage measurements and DTA analysis. DTA analysis on the A/W base glass, revealed two crystallisation peaks at about 1150 and 1193 K, corresponding to the crystallisation of oxyapatite and β-wollastonite phases, respectively. The two corresponding activation energies, calculated with the Kissinger equation, were also reported.

The microstructure and the crystallinity of the A/W glass–ceramics were evaluated depending on the thermal treatment. The morphology and the microstructure were observed by SEM and the crystalline phases were detected by X-ray diffraction. Finally the porosity was determined via image analysis.

Keywords: Microstructure-final; Glass–ceramics; Biomedical applications; Coatings

1. Introduction

Bioactive glasses and glass–ceramics are widely studied due to their particular property of directly bonding to the human tissues by interfacial reactions. In fact some bioceramics, such as Bioglass®, glass–ceramic A/W and sintered hydroxyapatite, form bone-like apatite on their surfaces in the living body and bond to living tissues through the apatite layer.[1–6] Since they have poor mechanical properties, in particular low fracture toughness, they are not suitable for load bearing applications and many efforts have been addressed to use them as coatings onto metallic materials such as stainless steel, Co–Cr–Mo alloys and titanium alloys.[7] Different coating techniques have been introduced such as dip coating, electrophoretic deposition, sintering, hot isostatic pressing, flame spraying and plasma spraying.[8,9] In the plasma spraying technique, the coating material in powder form is inserted into a plasma flux, where it is accelerated and heated up to fusion. The melted particles impact against the substrate and flatten on it, solidifying in a few microseconds and assuming a typical lamellar morphology.[10–13] Because of the high temperature in the plasma, the technique is particularly useful for spraying ceramics. Among osteoconductive plasma-sprayed coatings that can be used in orthopaedic surgery, it is worth citing hydroxyapatite, calcium phosphate and, more recently, bioactive glasses and glass–ceramics. HA plasma-sprayed coatings are widely used in biomedical

* Corresponding author. Tel.: +39 059 2056236; fax: +39 059 2056243.
E-mail address: cristina.siligardi@unimore.it (C. Siligardi).

0955-2219/$ – see front matter © 2008 Elsevier Ltd. All rights reserved.
doi:10.1016/j.jeurceramsoc.2008.06.034

applications,[14–19] while only a few studies concern plasma-spraying of glass–ceramics. The HA-coated implants still have some serious drawbacks resulting in significant challenges in their expanded utilisation.[20] Moreover, there were some attempts to deposit bioactive glass coatings, also in combination with HA,[20–31] but to the best of the authors' knowledge, the A/W glass–ceramic has not been deposited by plasma spraying up to date.

Among bioactive ceramics, the A/W glass–ceramic studied by Kokubo in 1980s[32–40] shows high bioactivity and high mechanical strength compared to other glasses and glass–ceramics. Such an high mechanical strength is attributed to the relatively high fracture toughness due to the precipitation of β-wollastonite in addition to apatite.[35] Kokubo *et al.*[34] found also that crystallisation of the parent glass in a bulk form led to the occurrence of large cracks in the crystallised sample while crystallisation of the same glass in a powder compact led to the formation of a crack-free dense crystallised sample. It was attributed to the uniform crystallisation of apatite and wollastonite in the sample obtained from the compact powders. Moreover, A/W glass–ceramics are one of the most bioactive materials: in fact it has been reported that the bioactivity index of the A/W glass–ceramic is slightly higher than that of dense sintered hydroxyapatite: in fact the bioactivity index of the A/W glass–ceramic is 3.2, while the bioactivity index of the hydroxyapatite is 3.[5,6] This means that the A/W glass–ceramic is more bioactive and requires less time for bone bonding in comparison with hydroxyapatite.

Hence, plasma-sprayed bioactive glass–ceramic coatings could potentially be used in orthopaedic implants, such as hip prosthesis, instead of hydroxyapatite.

Since the type of crystals formed in the A/W glassy matrix are determined by the thermal treatment,[41–43] a post-process thermal treatment of the sprayed coating is necessary, in order to obtain the required crystalline phases and to increase the coating mechanical properties.

Following a previous research,[44] in this study A/W glass–ceramic powders, obtained from industrial raw materials, were plasma-sprayed onto Ti–6Al–4V substrates. To the best of the authors' knowledge, this study is the first attempt to thermally spray the A/W glass ceramics onto a titanium alloy for potential biomedical applications, thus coupling the toughness of the substrate with the bioactivity of the coating. This could be a valuable alternative to commercial HAp-coated titanium implants: since, as mentioned, the A/W glass–ceramic is more bioactive (i.e. higher bioactivity index) than commercial HA and has better mechanical properties.[2]

Controlling the crystallisation of the glass–ceramic might be difficult, if pores and defects are present in the microstructure.[11,45] In fact, the peculiar microstructure of the plasma-sprayed coatings might have a significant influence on the crystallisation behaviour of the system. In order to enhance the A/W coatings microstructure, thermal treatments on A/W plasma-sprayed coatings and on A/W bulk and sintered samples of the same composition were analysed. Such comparison with bulk and sintered A/W could be useful for evaluating conventional alternatives for producing low cost coatings (e.g. via a glazing technique).

2. Materials and methods

The glass composition labelled A/W and reported by Kokubo *et al.*[32–39] was chosen as the reference composition and is shown in Table 1. The batch mixtures were prepared by using SiO_2, $MgCO_3$, $CaCO_3$, $Ca_3(PO_4)_2$ and CaF_2 raw materials. The A/W frit, of the same composition as that reported in a previous work,[44] was obtained using industrial raw materials and was labelled AWC.

Frits were obtained by quenching the glass in water while a bulk sample was obtained by pouring the melt onto a graphite mould. The frits were milled with a fast planetary moving mill, with sintered alumina balls in dry conditions, obtaining two different grain size distributions: fine (average particles diameter of about 15 μm) and coarse (average diameter in the 75–100 μm range) suitable for sintering and plasma-spraying, respectively. The coarse one was chosen for reaching a good flowability in the plasma-spray equipment.

The glass powders were subjected to chemical analysis (ICP-AES, Varian, Liberty 200), in order to evaluate the real chemical composition of the frit.

In order to better characterise the base glass, several mechanical, physical and thermal properties were measured. The as-cast glasses were then annealed at 1033 K for 1 h, in order to relax internal stress induced by fast cooling. The bulk glass samples were cut, obtaining 15 mm × 15 mm × 20 mm bars. Dilatometry (DIL 404, Netzsch) was performed on 15 mm × 5 mm × 5 mm bars obtained from bulk samples by cutting and grinding.

A crystallisation study was performed on bulk samples in an electric furnace. The heating rate was 10 K/min in all cases. Crystallisation isotherms at 1073, 1123, 1173, 1223, and 1273 K for 30 min were performed. Samples were cooled to room temperature inside the kiln after heat treatment. Heat-treated samples cross-sections were observed by scanning electron microscopy (ESEM Quanta-200 coupled with EDS Oxford INCA 350). The bulk samples were also crushed and ball milled (in agate jar with agate balls), and the resulting powders were

Table 1
Nominal composition of A/W and real composition of AWC in oxides (wt%)

Composition (wt%)	SiO_2	P_2O_5	CaO	CaF_2	Al_2O_3	MgO	Others
Nominal composition of A/W[9]	34	16.2	44.7	0.5	–	4.6	–
Real composition of AWC[44]	33.30	13.30	48.20	0.03	1.90	1.92	1.35

Table 2
Plasma torch operating parameters[44]

Operating parameters	
Ar flow (slpm)	47.4
H_2 flow (slpm)	8.5
Current (A)	550
Voltage (V)	64.9
Feed rate (rpm)	15
Nozzle diameter (mm)	8
Spraying distance (mm)	70

subjected to X-ray powders diffractometry (XRD, PW 3710, Philips).

The AWC powders were plasma-sprayed on Ti–6Al–4V substrates using a system equipped with a F4MB torch, in APS mode, using the operating parameters listed in Table 2.

The substrates of Ti–6Al–4V, having dimensions of 10 mm × 3 mm × 180 mm, were grit blasted with alumina particles before deposition.

Following literature indications,[46] fine powders, obtained through sieving the milled powders with a 38 μm sieve, were employed for the Differential Thermal Analysis (DTA). DTA analysis (Netzsch DSC 404 differential thermal analyzer) was performed by using 30 mg of powders heated from 283 to 1673 K at 10 K/min, in order to obtain the critical temperatures of the frits, such as glass transition, crystallisation and melting temperatures (T_g, T_p, T_m). Furthermore, to determine the kinetics parameters for the crystallisation, the temperatures T_{p_1} and T_{p_2}, corresponding to the maximum of the crystallisation peaks were determined at different heating rates, Φ, at 5, 10, 15 and 20 K/min. The error in the determination of the maximum position was primarily due to the accuracy of DTA, which is ±2 K. AWC crystallisation activation energy (E_a) was determined according to Kissinger's equation.[46–48]

In order to improve the microstructure and the mechanical properties of the as-sprayed AWC coatings, thermal treatments were performed in an electric furnace to sinter and crystallise the coatings. Previous studies [49,50] demonstrated that thermal treatments were necessary in order to enhance the microstructure of the plasma-sprayed coatings and to transform the layer from a glass into a glass–ceramic, inducing the sintering and the nucleation and growth of crystals. The heating rate was 10 K/min in all cases. Thermal treatments at 1048, 1073, 1098, 1123, 1173 and 1223 K for 1 h were performed on the coatings. Furthermore, thermal treatments at 1123, 1173 and 1223 K for 30 min were performed on the coatings in order to evaluate the effect of the time of the crystallisation isotherm on the nucleation and growth of crystals. All the samples were cooled to room temperature inside the furnace after heat treatments. The as-sprayed and the thermally treated coatings characterisation was performed by scanning electron microscopy (ESEM Quanta-200, coupled with EDS Oxford INCA 350)—both in surface and in cross-section (mounted in resin, ground with 800, 1000, and 2000 mesh SiC papers and polished with 3 and 0.5 μm poly-crystalline diamond suspension). X-ray diffraction analysis (X'PERT PRO), from 15° to 70° 2θ at a speed of 2°/min with 0.02° increment, using Cu Kα at 40 kV and 40 mA, was performed on the coatings surfaces. The average porosity was evaluated on SEM cross-section images via an image analysis software.

The crystallisation study was also carried out on the sintered samples. The finer glass powders were wetted with 6 wt% of distilled water and uniaxially pressed in 40 mm diameter disks under a 29 bar load. The pressed disks were sintered and crystallised in an electric furnace, using the same thermal cycles described above (10 K/min heating rate, isotherm at 1073, 1123, 1173, 1223, and 1273 K for 30 min, slow cooling). The linear shrinkage (%) of samples was also measured. Cross-sectional samples from sintered disks were observed by SEM. The cross-sections were attached 5 s with HCl 1N and washed with bidistilled water, in order to remove part of the glassy matrix and to better observe the crystals. The powders obtained by crushing and milling the samples (as for the bulk glass samples) were also subjected to X-ray diffractometry. As for the plasma-sprayed samples, the porosity was evaluated with an image analysis software from SEM cross-sections.

3. Results and discussion

3.1. Powders characterisation

The chemical analysis of the studied glass powders (labelled AWC) is reported in Table 1: it is worth noting that Al_2O_3 was present in the frit in the amount of about 1.90%, due to the not pure raw materials used and to the milling. The XRD spectrum confirmed that the milled frit was vitreous (Fig. 1).

The AWC powders used for thermally spraying had a coarse particle size distribution, with a particle size distribution in the 75–100 μm range, while the dry milled AWC powders used for sintered samples had a finer particle distribution, with a D_{50} = 15 μm and D_{90} = 40 μm. Differential thermal analyses indicated that the AWC glass had a T_g at around 993 K (Fig. 2), two exothermal peaks, T_{p_1} and T_{p_2}, at around 1160 and 1200 K and two endothermic peaks, T_{m_1} and T_{m_2}, at around 1503 and 1557 K. Two exothermal peaks correspond to the crystallisation of apatite (oxyapatite JCPDS 89-6495) at β-wollastonite

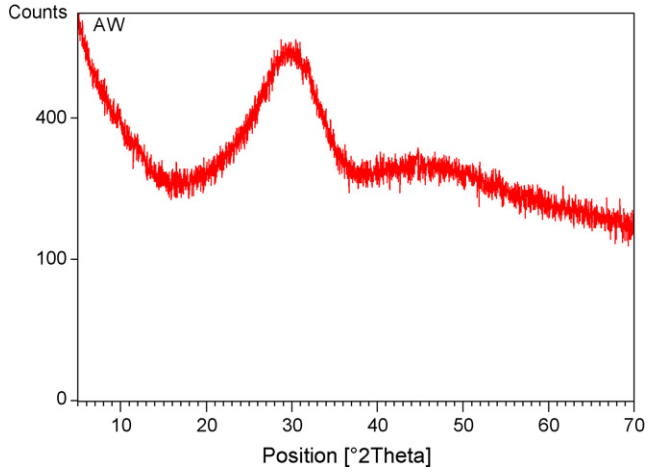

Fig. 1. XRD pattern of AWC powder.

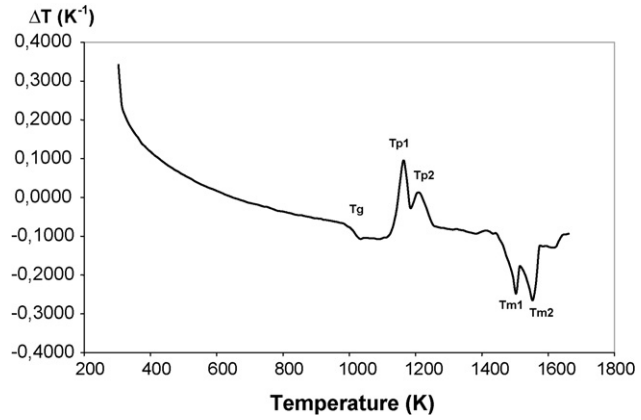

Fig. 2. Differential thermal analysis of AWC glass (heating rate 10 K/min).

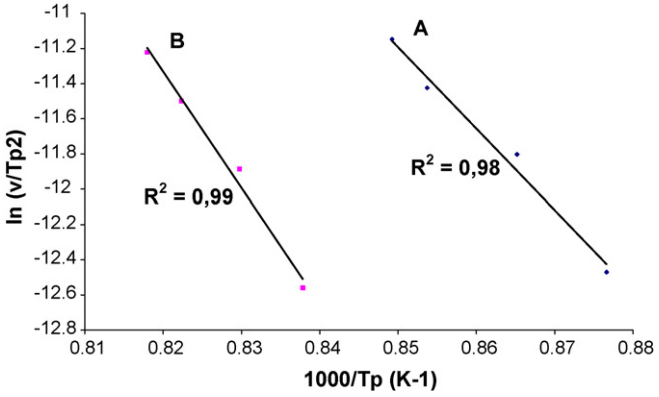

Fig. 3. Kissinger's equation plot: (A) first peak of crystallisation and (B) second peak of crystallisation.

crystals, respectively, while two endothermic peaks may be attributed to the melting of two crystalline phases.

The position of the first crystallisation peak, labelled T_{p_1}, varied between 1150 and 1177 K when the heating rate was increased from 5 to 20 K/min. The position of the second crystallisation peak, labelled T_{p_2}, varied between 1193 and 1212 K when the heating rate was increased from 5 to 20 K/min. Fig. 3 shows the corresponding Kissinger plot, from which the slopes ($-E/R$) were calculated by least squares fitting of the data straight line. The calculated E represents the activation energy

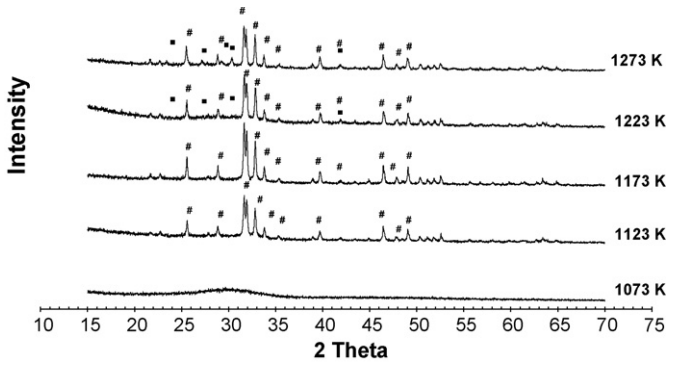

Fig. 4. XRD pattern of bulk AWC glasses after different thermal treatments (legend: (#) oxyapatite JCPDS 89-6495; (■) wollastonite JCPDS 42-0550).

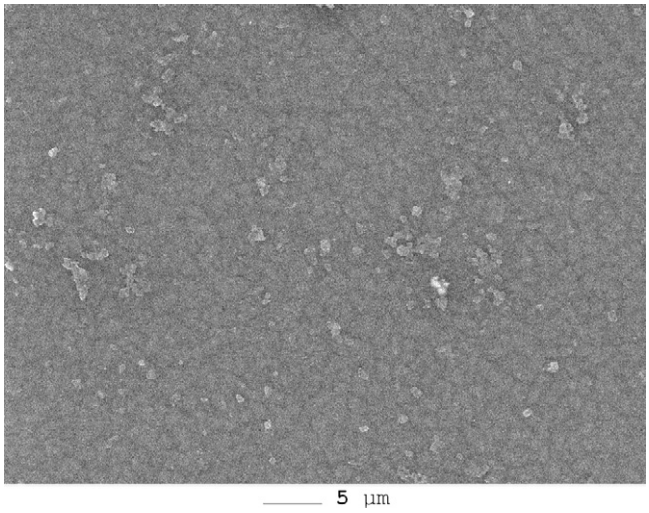

Fig. 5. SEM micrographs of AWC bulk glasses thermal treated at 1223 K.

for combined crystal nucleation and growth because no prior nucleation heat treatment was performed in this study. The activation energy for crystallisation of the first exoterm (i.e. apatite phase) was 385 ± 11 kJ/mol, and that of the second exotherm (i.e. wollastonite phase) was 550 ± 16 kJ/mol. The results are

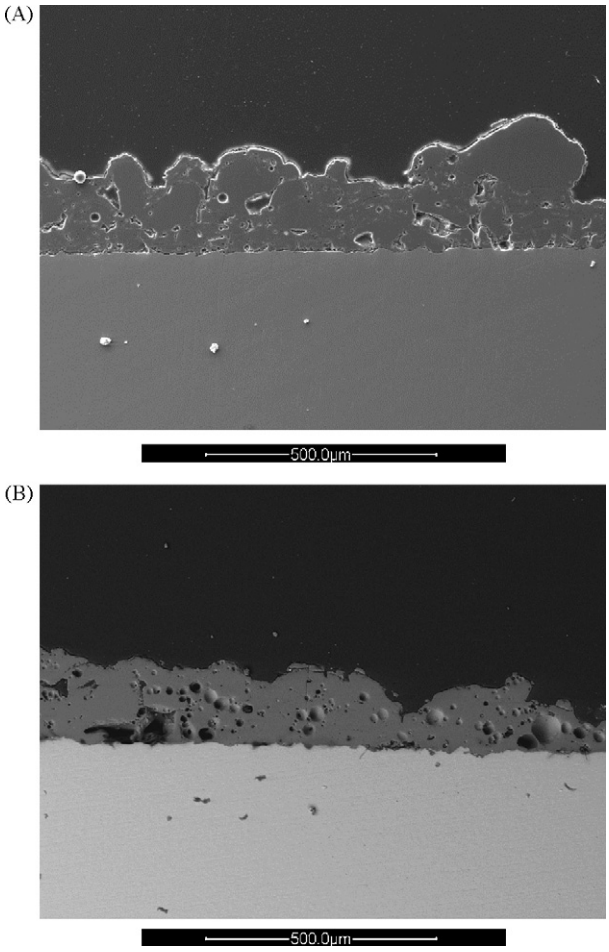

Fig. 6. SEM cross-section of AWC as-sprayed (A) and thermally treated at 1173 K (B).

in contrast with the data reported in[51] (since this work reported a wollastonite activation energy – about 374 kJ/mol lower than the apatite one – about 514 kJ/mol), but are closer to the data reported in[52] (the authors reported an activation energy of 447 kJ/mol at $T_p = 1220$ K that corresponds to wollastonite crystallisation). In fact, the glass investigated in[51] had a chemical composition similar to the glass studied in this paper even if the CaF_2 content was higher than in the AWC glass, and alumina was absent. Probably small differences in the composition could change the kinetic parameters of the crystallisation. In fact Calver *et al.*[53] showed that different amount of fluorine could modify several properties (i.e. viscosity, melting point, sintering process, etc.) so consequently also the crystallisation behaviour of the glass.

3.2. Bulk glass samples characterisation

Since the AWC glass powder characterisation might be difficult, the mechanical and physical properties of the bulk glass were evaluated. This was necessary in order to have a complete characterisation of the base glass before its thermal spraying onto the Ti–6Al–4V substrates.

The bulk glass had a density of 2.9172 ± 0.0003 g/cm^3. The AWC glass density was higher in comparison with others glasses, such as borosilicate glasses, soda-lime glasses and high silica glasses, with a density of 2.23, 2.40, and 2.18 g/cm^3, respectively.[54]

The coefficient of thermal expansion, CTE ($323\,K < T < 673\,K$) of the AWC glass was $10 \times 10^{-6}\,K^{-1}$ similar to the CTE of the substrate ($9 \times 10^{-6}\,K^{-1}$) in order to avoid a delamination effect between the coating and the substrate. The Young's modulus of AWC glass was 78.3 GPa and the Poisson's ratio 0.33. The value of the Young's modulus can be influenced by the type of modifiers and intermediates present. Glasses containing Mg^{2+} as modifier, rather than Na^{2+}, have higher modulus. The presence of Al_2O_3, which has a high modulus in its crystalline state, also leads to high-modulus in glasses. Young's modulus of most commercial silicate glasses varies from about 50 GPa for low-T_g glasses to about 75 GPa for fused SiO_2 and E-glasses fibers. The AWC glass had therefore a high Young's modulus, in comparison with borosilicates (60–63 GPa), soda-lime silicates (66 GPa) and aluminosilicates (75 GPa).[54]

The XRD spectra of the thermal treated bulk AWC glass are reported in Fig. 4. After the thermal treatment at 1123 K only the apatite crystals (oxyapatite, labelled OHA, JCPDS 89-6495) were detected with XRD. The β-wollastonite crystals (labelled W, JCPDS 042-0550) appeared at 1223 K and the W

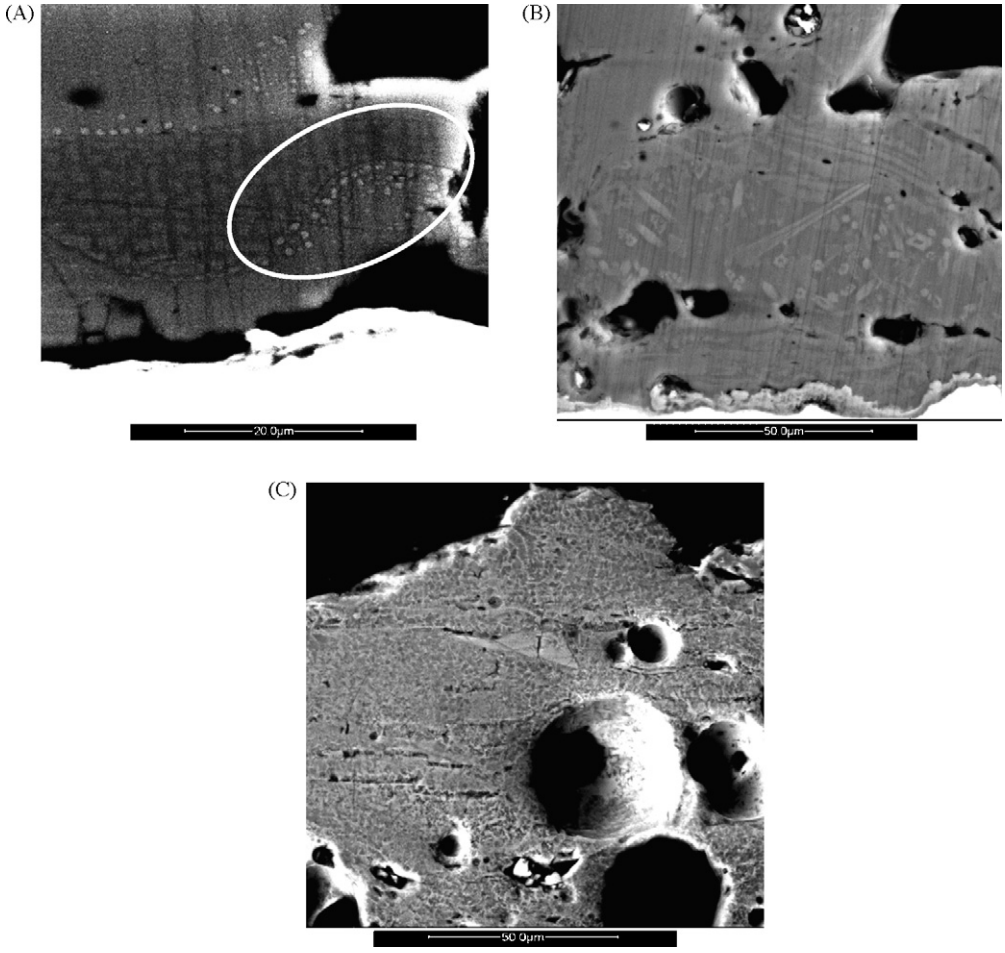

Fig. 7. SEM cross-section of thermally treated AWC coatings at: (A) 1048 K, (B) 1098 K, and (C) 1223 K.

Table 3
Average porosity of the as-sprayed and thermally treated AWC coatings

Temperature (K) of thermal treatments on AWC plasma-sprayed coatings	Average porosity (%)
As-sprayed	13.1 ± 2.1
1073	11.3 ± 2.0
1123	7.6 ± 0.4
1173	6.8 ± 1.3
1223	7.0 ± 0.9

peaks increased at increasing temperatures. The precipitation of apatite and β-wollastonite crystals was coherent with the DTA analysis, since the first crystallisation peak was at about 1150 K and the second one at about 1200 K. The crystals were detected with XRD but they were so small that SEM observations did not clearly reveal their morphology (Fig. 5).

3.3. Coatings characterisation

The as-sprayed AWC coating had an average thickness of about 180 μm and an average porosity of 13.1 ± 2.1%, as determined from image analysis (Fig. 6A) and presented an highly defective microstructure with unmelted or partially melted particles, pores and cracks. After the different thermal treatments sintering took place, since the pores became rounded and a lot of cracks were closed. The porosity values are reported in Table 3: the porosity decreased to 7.6 ± 0.4% after the thermal treatment at 1123 K, reaching a value of about 6.8 ± 1.3% after the thermal treatment at 1173 K for 1 h (Fig. 6B). The surface roughness was not significantly changed after the thermal treatments. The interfaces between thermally treated coatings and substrates were quite good, even if after some thermal treatments a TiO_2 interlayer was formed, which caused a lot of cracks. A very fine crystallisation occurred during thermal treatments: after the thermal treatment at 1048 K some little crystals could be observed (as shown in Fig. 7A, see circle). After the thermal treatments at 1073 and 1098 K the crystals became larger (Fig. 7B). After the thermal treatment at 1173 K and 1223 K the coating was crystallised, as shown in Fig. 7C. The time of thermal treatment affected the crystallisation process: in fact in the case of the thermal treatment at 1123 K for 30 min (Fig. 8A) the sample showed a very fine microstructure (very small crystals were visible) while after 1 h the crystals were larger and well noticeable (Fig. 8B).

The XRD results are reported in Fig. 9. The as-sprayed AWC coating was glassy, as already reported in previous studies about plasma sprayed glass coatings.[11,50] After heat treatment, in these samples, the main crystalline phases were similar to those present in the bulk samples (oxyapatite and β-wollastonite) even if a new crystalline phase, diopside (labelled D), was detected in the sample treated at 1123 K.

3.4. Sintered glass samples characterisation

AWC sintered samples starting from pressed glass powders were also characterised and compared with plasma-sprayed

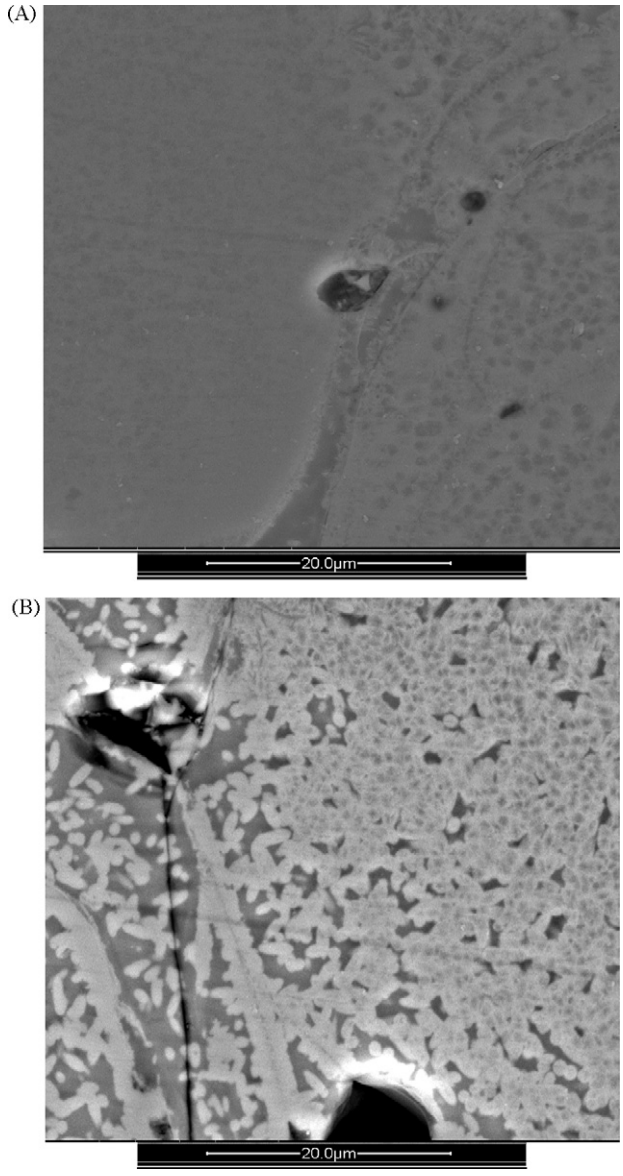

Fig. 8. SEM cross-section of AWC thermally treated at 1123 K: (A) for 30 min and (B) for 1 h.

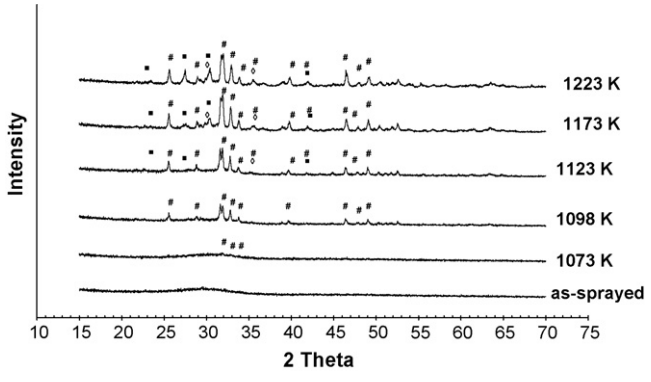

Fig. 9. XRD pattern of AWC coating as-sprayed and after different thermal treatments (legend: (#) oxyapatite JCPDS 89-6495; (■) wollastonite JCPDS 42-0550; (◊) diopside JCPDS 17-0318).

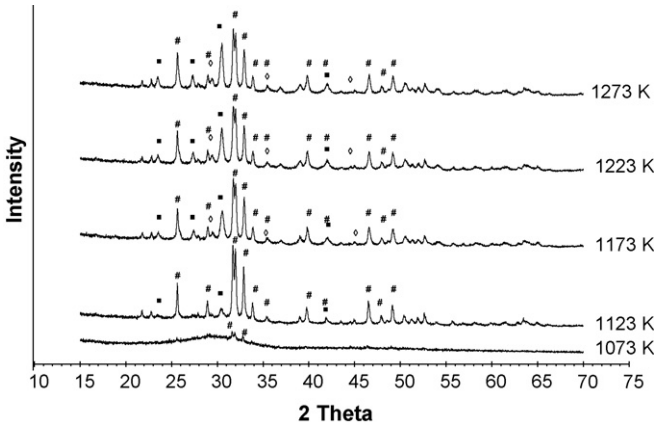

Fig. 10. XRD pattern of sintered AWC glass after different thermal treatments. (Legend: (#) oxyapatite JCPDS 89-6495; (■) wollastonite JCPDS 42-0550; (◊) diopside JCPDS 17-0318).

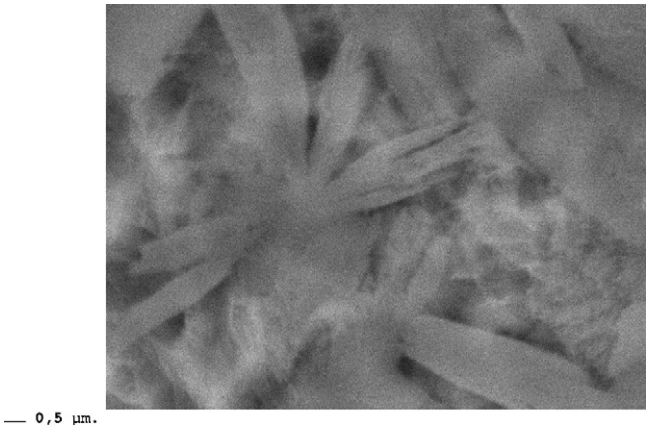

Fig. 12. SEM cross-sections of sintered AWC after thermal treatment of 1123 K, after a chemical etching with HCl 1N.

samples. The XRD pattern is shown in Fig. 10. Oxyapatite, wollastonite and diopside were the main phases also in these samples. After the thermal treatment at 1073 K, traces of oxyapatite were detected, while wollastonite crystals appeared after the thermal treatment at 1123 K. Diopside crystals appeared at a higher temperature (1173 K).

Fig. 11 shows the SEM cross-sections of AWC sintered glass thermally treated at 1073, 1173 and 1273 K. The glasses seemed to be sintered but no crystals were visible with SEM (Fig. 11A–C). Only after a chemical etching with HCl 1N for 5 s on the sintered sample thermally treated at 1123 K some small crystals were detected (Fig. 12).

Table 4
Average porosity of the as-sintered and thermally treated AWC sintered samples

Temperature of sintering (K)	Average porosity (%)
As-sintered	25.3 ± 1.6
1073	6.7 ± 0.3
1123	5.3 ± 0.3
1173	3.2 ± 0.1
1223	3.2 ± 0.5
1273	3.3 ± 0.2

The residual porosity decreased after the thermal treatment at 1173 K as reported in Table 4: in fact the sintered samples showed a porosity of 25.2 ± 1.6%, reaching at 1173 K an average value of 3.2 ± 0.1%. In order to explain this residual porosity

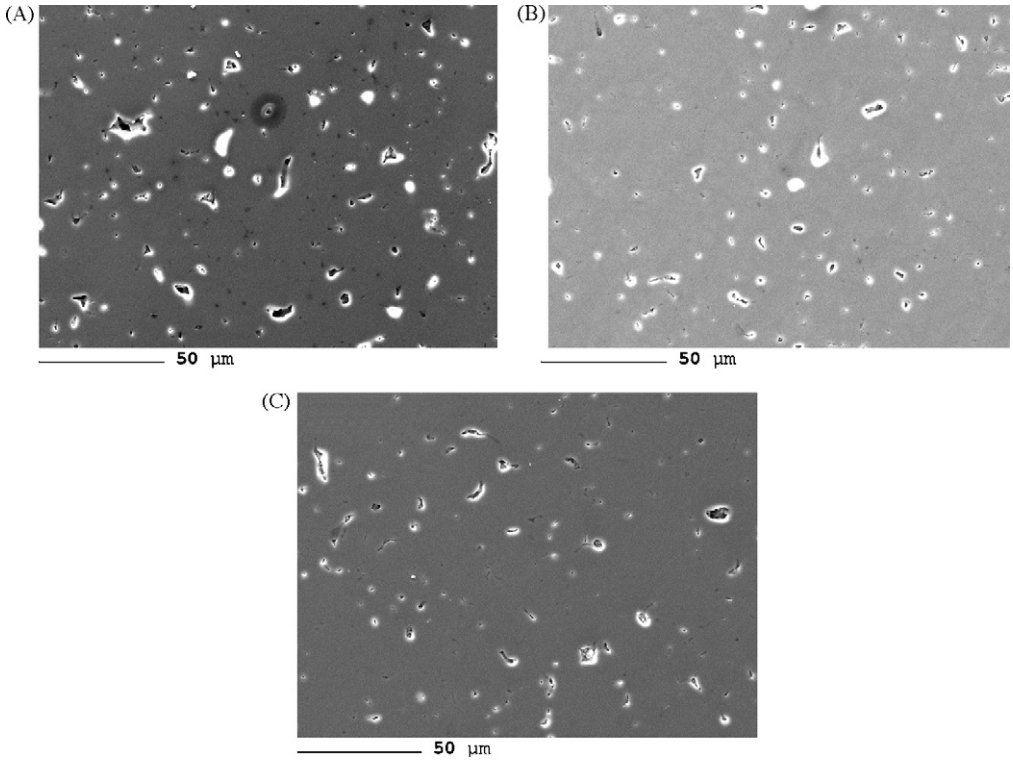

Fig. 11. SEM cross-sections of sintered AWC after thermal treatments of: (A) 1073 K, (B) 1173 K, and (C) 1273 K.

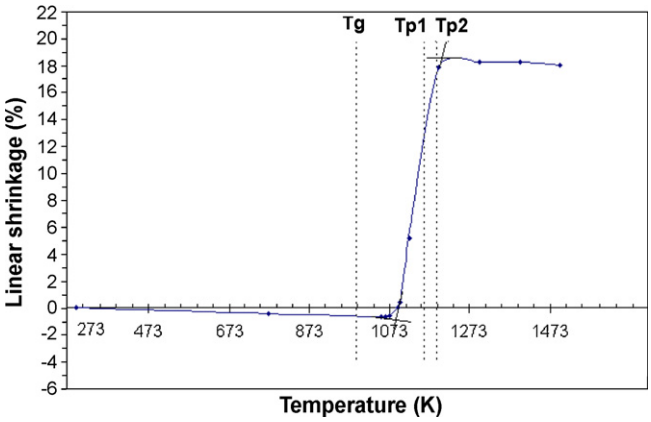

Fig. 13. Linear shrinkage of the sintered AWC sample.

shown by sintered and coating samples, the linear shrinkage of the AWC glass versus temperature is shown in Fig. 13; T_g, and T_p temperatures were reported in the same graph. The first and final sintering shrinkage temperatures were obtained by means of intersections between the linear fit in the temperature range $1000\,K \leq T \leq 1300\,K$. The thermal shrinkage curve indicated that the glass powders compact started to densify at about 1079 K and ended at about 1205 K. A previous study[55] demonstrated that is useful to compare, on the same temperature scale, DTA and linear shrinkage plots to determine how composition may affect sintering and devitrification processes. In AWC glass the T_g fell before the first sintering shrinkage temperature and the crystallisation temperatures (T_{p_1} and T_{p_2}) fell before the maximum densification plateau, as reported in Fig. 13. This study demonstrated that the crystallisation process started before complete densification was achieved. These results could explain why both coatings and sintered samples showed a relevant porosity after heating.

4. Conclusions

In this study, apatite/wollastonite thermally sprayed glass–ceramics coatings were investigated and the results were compared with sintered glass–ceramics obtained via a conventional method.

The crystalline phases formed after specific thermal treatments were mainly oxyapatite and wollastonite, in all glass–ceramics. However, bulk samples required higher thermal treatment temperatures with respect to sintered and plasma-sprayed samples to develop a significant amount of crystalline phases.

The microstructure of the AWC as-sprayed coatings possessed a lot of defects, such as pores and micro-cracks. During the thermal treatments a lot of cracks were closed, but not enough to reach a remarkably lower value of porosity, since sintering and crystallisation occurred simultaneously as happened also in the sintered samples. Therefore, the thermal treatments were not able to significantly enhance the microstructure of the plasma-sprayed coatings but they were necessary in order to obtain the precipitation of crystalline phases in the glassy matrix, as detected by SEM. The time of the thermal treatments affected the amount and the size of crystals formed in the coatings.

From this preliminary investigation it seems feasible to obtain coatings both via plasma spraying and via a conventional route (e.g. a glazing technique), even if the processes require further optimisation.

Acknowledgments

The authors would like to thank Nadja Cozminca, University of IASI (Romania), for her help in characterising sintered samples. Ravi Kumar (Indian Institute of Technology, Kanpur) is acknowledged for his help in performing the thermal treatments on AWC coatings. Prof. Sampath acknowledges partial support from the National Science Foundation for this work under award CMMI-0605704.

References

1. Cao, W. and Hench, L. L., Bioactive materials. *Ceramics International*, 1996, **22**, 493–507.
2. Hench, L. L., Bioceramics. *Journal of American Ceramic Society*, 1998, **81**, 1705–1728.
3. Hench, L. L., Bioceramics, a clinical success. *American Ceramic Society Bulletin*, 1998, **7**, VII.
4. Hench, L. L., Bioceramics: from concept to clinic. *Journal of American Ceramic Society*, 1991, **74**, 1487–1510.
5. Ratner, B. D., Hoffman, A. S., Schoen, F. J. and Lemons, J. E., Biomaterials science. *An Introduction to Materials in Medicine*. Elsevier Academic Press, 2004.
6. De AZa, P. N., De Aza, A. H., Pena, P. and De Aza, S., Bioactive glass and glass–ceramics. *Ceramica y Vidro, Bolletin Sociedad Espanola Ceramica*, 2007, **46**(2), 45–55.
7. Liang, H., Shi, B., Fairchild, A. and Cale, T., Application of plasma coatings in artificial joints: an overview. *Vacuum*, 2004, **73**, 317–326.
8. Sun, L., Berndt, C. C., Gross, K. A. and Kucuk, A., Material fundamentals and clinical performance of plasma-sprayed hydroxyapatite coatings: a review. *Journal of Biomedical Materials Research*, 2001, **58**, 570–592.
9. Zhao, Y., Chen, C. and Wang, D., The current techniques for preparing Bioglass coatings. *Surface Review and Letters*, 2005, **12**(4), 505–513.
10. Heimann, R., Thermal spraying of biomaterials. *Surface and Coatings Technology*, 2006, **201**, 2012–2019.
11. Bolelli, G., Lusvarghi, L., Manfredini, T. and Siligardi, C., Influence of the manufacturing process on the crystallisation behaviour of a CZS glass system. *Journal of Non-Crystalline Solids*, 2005, **351**, 2537–2546.
12. Pasandideh-Fard, M., Chandra, S. and Mostaghimi, J., A three-dimensional model of droplet impact and solidification. *International Journal of Heat and Mass Transfer*, 2002, **45**, 2229–2242.
13. Bianchi, L., Denoirjean, A., Blein, F. and Fauchais, P., Microstructural investigation of plasma-sprayed ceramic splats. *Thin Solid Films*, 1997, **299**, 125–135.
14. Kweh, S. W. K., Khor, K. A. and Cheang, P., Plasma-sprayed hydroxyapatite (HA) coatings with flame-spheroidized feedstock: microstructure and mechanical properties. *Biomaterials*, 2000, **21**, 1223–1234.
15. Guipont, V., Espanol, M., Borit, F., Llorca-Isern, N., Jeadin, M., Khor, K. A. *et al.*, High-pressure plasma spraying of hydroxyapatite powders. *Materials Science and Engineering A*, 2002, **325**, 9–18.
16. Espanol, M., Guipont, V., Khor, K. A., Jeadin, M. and Llorca-Isern, N., Effect of heat treatment on high pressure plasma sprayed hydroxyapatite coatings. *Surface Engineering*, 2002, **18**(3), 213–218.
17. Deram, V., Minichiello, C., Vannier, R. N., Le Maguer, A., Pawlowski, L. and Murano, D., Microstructural characterizations of plasma sprayed hydroxyapatite coatings. *Surface and Coatings Technology*, 2003, **166**, 153–159.
18. Dyshlovenko, S., Pateyron, B., Pawlowski, L. and Murano, D., Numerical simulation of hydroxyapatite powder behaviour in plasma jet. *Surface and Coatings Technology*, 2004, **179**, 110–117.

19. Lu, Y., Xiao, G., Li, S., Sun, R. and Li, M., Microstructural inhomogeneity in plasma-sprayed hydroxyapatite coatings and effect of post-heat treatment. *Applied Surface Science*, 2006, **252**(6), 2412–2421.
20. Schrooten, J. and Helsen, J. A., Adhesion of bioactive glass coating to Ti–6Al–4V oral implant. *Biomaterials*, 2000, **2**, 1461–1469.
21. Goller, G., The effect of bond coat on mechanical properties of plasma sprayed Bioglass-titanium coatings. *Ceramics International*, 2004, **30**, 351–355.
22. Goller, G., Oktar, F. N., Yazici, T., Gurmen, S. and Kayali, E. S., Characterization of plasma sprayed Bioglass coatings on titanium. *Key Engineering Materials*, 2003, **240–242**, 283–286.
23. Vernè, E., Ferraris, M., Jana, C. and Baracchini, L., Bioverit® I base glass/Ti particulate biocomposite: "in situ" vacuum plasma spray deposition. *Journal of the European Ceramic Society*, 2000, **20**, 473–479.
24. Vernè, E., Bona, E., Angelini, E., Rosalbino, F. and Appendino, P., Correlation between microstructure and properties of biocomposite coatings. *Journal of the European Ceramic Society*, 2002, **22**, 2315–2323.
25. Chern Lin, J. H., Lin, H. J., Ding, S. J. and Ju, C. P., Characterization of immersed hydroxyapatite–bioactive glass coatings in Hank's solution. *Materials Chemistry and Physics*, 2000, **64**, 229–240.
26. Carvalho, F. L. S., Borges, C. S., Branco, J. R. T. and Pereira, M. M., Structural analysis of hydroxyapatite/bioactive glass composite coatings obtained by plasma spray processing. *Journal of Non-Crystalline Solids*, 1999, **247**, 64–68.
27. Lee, T. M., Chang, E., Wang, B. C. and Yang, C. Y., Characteristics of plasma-sprayed bioactive glass coatings on Ti–6A1–4V alloy: an in vitro study. *Surface and Coatings Technology*, 1996, **79**, 170–177.
28. Gabbi, C., Cacchioli, A., Locardi, B. and Guadagninol, E., Bioactive glass coating: physicochemical aspects and biological findings. *Biomaterials*, 1995, **16**, 515–520.
29. Silva, P. L., Santos, J. D., Monteiro, F. J. and Knowles, J. C., Adhesion and microstructural characterization of plasma-sprayed hydroxyapatite/glass ceramic coatings onto Ti–6A1–4V substrates. *Surface and Coatings Technology*, 1998, **102**, 191–196.
30. Ding, S. J., Ju, C. P. and Chern Lin, J. H., Morphology and immersion behavior of plasma sprayed hydroxyapatite/bioactive glass coatings. *Journal of Materials Science: Materials in Medicine*, 2000, **11**, 183–190.
31. Bessmertnyi, V. S., Krokhin, V. P., Panasenko, V. A., Drizhd, N. A., Dyumina, P. S. and Kolchina, O. M., Plasma rod decorating of household glass. *Glass and Ceramics*, 2001, **58**, 214–215.
32. Kitsugi, T., Yamamuro, T., Nakamura, T. and Kokubo, T., Bone bonding behaviour of $MgO–CaO–SiO_2–P_2O_5–CaF_2$ glass (mother glass of A/W glass–ceramics). *Journal of Biomedical Materials Research*, 1989, **23**, 631–648.
33. Kokubo, T., Ito, S., Huang, T., Hayashi, T., Sakka, S. and Kitsugi, T., CaP-rich layer formed on high-strength bioactive glass–ceramic A–W. *Journal of Biomedical Materials Research*, 1990, **24**, 331–343.
34. Kokubo, T., Ito, S., Sakka, S. and Yamamuro, T., Formation of a high strength bioactive glass–ceramic in the system $MgO–CaO–SiO_2–P_2O_5$. *Journal of Materials Science*, 1986, **21**, 536–540.
35. Kokubo, T., Bioactive glass ceramics: properties and applications. *Biomaterials*, 1991, **12**, 155–163.
36. Nakamura, T., Yamamuro, T., Higashi, S., Kokubo, T. and Ito, S., A new glass–ceramic for bone replacement: evaluation of its bonding to bone tissue. *Journal of Biomedical Materials Research*, 1985, **19**, 685–698.
37. Kitsugi, T., Yamamuro, T. and Kokubo, T., Bonding behaviour of a glass–ceramic containing apatite and wollastonite in segmental replacement of the rabbit tibia under load-bearing conditions. *The Journal of Bone and Joint Surgery*, 1989, **71**(2), 264–272.
38. Yoshi, S., Kakutani, Y., Yamamuro, T., Nakamura, T., Kitsugi, T., Oka, M. *et al.*, Strength of bonding between A–W glass–ceramic and surface of bone cortex. *Journal of Biomedical Materials Research*, 1988, **22**, 327–338.
39. Kitsugi, T., Yamamuro, T., Nakamura, T. and Kokubo, T., The bonding of glass ceramics to bone. *International Orthopaedics*, 1989, **13**, 199–206.
40. Park, J. and Ozturk, A., Tribological properties of $MgO–CaO–SiO_2–P_2O_5$–F-based glass–ceramic for dental applications. *Materials Letters*, 2006, **61**, 1916–1921.
41. Chang, C. K., Mao, D. L. and Wu, J. S., Characteristics of crystals precipitated in sintered apatite/wollastonite glass ceramics. *Ceramics International*, 2000, **26**, 779–785.
42. Marghussian, V. K. and Sheikh-Mehdi Mesgar, A., Effects of composition on crystallization behaviour and mechanical properties of bioactive glass–ceramics in the $MgO–CaO–SiO_2–P_2O_5$ system. *Ceramics International*, 2000, **26**, 415–420.
43. Liu, D.-M. O., Bioactive glass–ceramic: formation, characterization and bioactivity. *Materials Chemistry and Physics*, 1994, **36**, 294–303.
44. Cannillo, V., Colmenares-Angulo, J., Lusvarghi, L., Pierli, F. and Sampath, S., In vitro characterisation of plasma-sprayed apatite/wollastonite glass–ceramic biocoatings on titanium alloys, Submitted.
45. Zanotto, E. D., Experimental studies of surface nucleation and crystallisation of glasses. *Ceramic Transactions*, 1993, **30**, 65.
46. Ray, C. S. and Day, D. E., Nucleation and crystallisation in glasses as determined by DTA. *Ceramic Transactions*, 1993, **30**, 207–223.
47. Ferrari, A. M., Leonelli, C., Pellacani, G. C. and Siligardi, C., Effect of V_2O_5 addition on the crystallisation of glasses belonging to the $CaO–ZrO_2–SiO_2$ system. *Journal of Non-Crystalline Solids*, 2003, **315**, 77.
48. Kissinger, H. E., Reaction Kinetics in Differential Thermal Analysis. *Analytical Chemistry*, 1957, **29**, 1702.
49. Bolelli, G., Lusvarghi, L., Manfredini, T. and Siligardi, C., Devetrification behaviour of plasma-sprayed glass coatings. *Journal of the European Ceramic Society*, 2006, **27**, 623–628.
50. Bolelli, G., Lusvarghi, L., Manfredini, T., Parsini, E. and Siligardi, C., BAS, CMAS and CZAS glass coatings deposited by plasma spraying. *Journal of the European Ceramic Society*, 2007, **27**, 4575–4588.
51. Likitvanichkul, S. and La Course, W., Apatite–wollastonite glass–ceramics. *Journal of Materials Science*, 1998, **33**, 5901–5904.
52. Yung, B., Liang, K., Hu, A. and Gu, S., Influence of different TiO_2 content on crystallization of $CaO–MgO–P_2O_5–SiO_2$ system glasses. *Material Letters*, 2002, **56**, 539–542.
53. Calver, A., Hill, R. G. and Stamboulis, A., Influence of fluorine content on the crystallization behaviour of apatite–wollastonite glass–ceramics. *Journal of Materials Science*, 2004, **39**, 2601–2603.
54. Rawson, H., Properties and applications of glasses. *Glass Science and Technology*, *vol. 3*. Elsevier, Amsterdam, 1980.
55. Siligardi, C., D'Arrigo, M. C. and Leonelli, C., Sintering behaviour of glass–ceramics frits. *American Ceramic Society Bulletin*, 2000, **79**, 88–92.